Bright Single InAsP Quantum Dots at Telecom Wavelengths in Position-Controlled InP Nanowires: The Role of the Photonic Waveguide

Sofiane Haffouz,*,[†] Katharina D. Zeuner,[‡] Dan Dalacu,[†] Philip J. Poole,[†] Jean Lapointe,[†] Daniel Poitras,[†] Khaled Mnaymneh,[†] Xiaohua Wu,[†] Martin Couillard,[†] Marek Korkusinski,[†] Eva Schöll,[‡] Klaus D. Jöns,[‡] Valery Zwiller,[‡] and Robin L. Williams[†]

[†]National Research Council of Canada, Ottawa, Ontario, Canada, K1A 0R6
[‡]KTH Royal Institute of Technology, Stockholm, 100 44 Sweden

S Supporting Information

ABSTRACT: We report on the site-selected growth of bright single InAsP quantum dots embedded within InP photonic nanowire waveguides emitting at telecom wavelengths. We demonstrate a dramatic dependence of the emission rate on both the emission wavelength and the nanowire diameter. With an appropriately designed waveguide, tailored to the emission wavelength of the dot, an increase in the count rate by nearly 2 orders of magnitude (0.4 to 35 kcps) is obtained for quantum dots emitting in the telecom O-band, showing high single-photon purity with multiphoton emission probabilities down to 2%.
Using emission-wavelength-optimized waveguides, we demonstrate bright, narrow-line-width emission from single InAsP quantum dots with an unprecedented tuning range of 880 to 1550 nm. These results pave the way toward efficient single-photon sources at telecom wavelengths using deterministically grown InAsP/InP nanowire quantum dots.

KEYWORDS: Quantum dot, nanowire, selective growth, vapor−liquid−solid, epitaxial growth, chemical beam epitaxy, photoluminescence, single-photon source
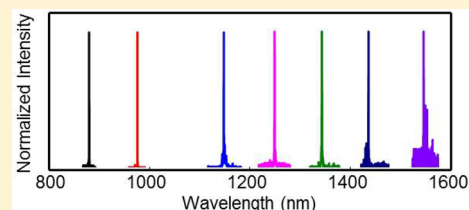
Nonclassical light sources that can produce streams of correlated on-demand photons are a central building block for optics-based quantum information technologies. In recent years, there has been a major drive to demonstrate single-photon sources for quantum key distribution (QKD) to provide secure communications over long distances. Sources for QKD need to generate single photons with a negligible probability of multiphoton emission, and for certain protocols, these photons need to be indistinguishable.[1,2] Ideally, the sources should produce single photons on demand at high repetition rates that can be efficiently collected by an external optical system.[3] Importantly, for fiber-based long-haul communications, the sources should emit photons with wavelengths in the telecom windows around 1.3 and 1.5 μm, at which point fiber losses are minimized. A broad tuning range is also desirable for free-space QKD, in which high transmission windows in the atmosphere exist at various wavelengths.

The InAs/InP quantum dot material system has been shown to emit efficiently at telecom wavelengths.[4,5] Single-photon emission at 1.5 μm was demonstrated in 2005,[6] and, more recently, bright single photon emission was demonstrated at 1.3 and 1.5 μm using photonic crystal cavities.[7,8] These devices were based on randomly nucleated quantum dots, although site-selected dots,[5,9] nucleated at specified positions on the substrate, are a preferred growth mode. Site selection opens up the possibility for deterministic integration of telecom quantum dots with photonic structures aimed at, for example, increasing device efficiency.[10]

The photonic nanowire approach to fabricating efficient quantum light sources has shown great promise, with demonstrated collection efficiencies of 72%.[11] Bottom-up based nanowire devices[12,13] are of particular interest because they can naturally contain one and only one dot per device and are readily grown using site-selective techniques.[14−16] Site-selected InAsP/InP nanowire quantum dot sources grown using a combined selective-area and vapor−liquid−solid (VLS) epitaxy approach[17] have demonstrated high collection efficiencies of 43% (corresponding to an 86% coupling into the fundamental HE_{11} nanowire waveguide mode) and near transform-limited line widths of 4 μeV.[18] Such sources can generate single photons with negligible multiphoton probabilities $(g_2(0) < 0.005)$[9] and polarization entangled photon pairs (via the biexciton−exciton cascade) with fidelities to the maximally entangled state exceeding 80%.[19−21] These sources utilize $InAs_xP_{1−x}$ quantum dots with $x \approx 30\%$ and operate at wavelengths of $\lambda \approx 950$ nm.

It is well-known that the diameter of the photonic nanowire will determine the spontaneous emission rate of the quantum

dot by affecting the available optical density of states, i.e., by dictating the overlap of the waveguide mode (e.g., HE_{11}) with the dipole field of the emitter.[22] Previous studies have shown an order of magnitude reduction in transition lifetimes[23] as well as more-modest increases in brightness[24] by optimizing the nanowire diameter. These studies tuned the photonic nanowire diameter and used dots emitting at a fixed energy. In this study, we first tune the quantum dot toward telecom wavelengths for a given nanowire diameter, producing a dramatic drop in emission intensity with increasing wavelength, and we then illustrate the recovery of the lost intensity by increasing the nanowire diameter at this longer wavelength. Using waveguides tailored to the emission wavelength of the dot, we demonstrate bright, narrow-line-width single-dot emissions tunable from $\lambda = 880$ nm up to $\lambda = 1550$ nm.

The devices used in this study consist of a nanowire core with one or two embedded InAsP quantum dots that are clad with an InP shell. The diameter of the core and of the dots is determined by the size of the gold catalyst particle (nominally, 18 nm for these studies), which is itself defined by electron-beam (e-beam) lithography. The diameter of the cladding, which defines the waveguide, is determined by the size of a circular opening in a SiO_2 mask defined by the time of a wet-etch step (see the Supporting Information). The top of the cladding is tapered to improve coupling to the external optical system.[25] Details of the device growth are given in refs 9. and 17.

To highlight the role of the waveguide design in determining the emission properties of the quantum dot emitters, we grew double quantum-dot samples (i.e., two dots in the same photonic nanowire waveguide) and varied the emission wavelength of one of the dots. A total of seven samples were grown with the two quantum dots incorporated in the nanowire core separated sufficiently to avoid any electronic coupling (see the inset of Figure 1a). The $InAs_xP_{1-x}$ quantum dot emission energy was tuned by controlling the dot composition, x through variation of the arsine flux. For the first dot (dot 1) the growth conditions were the same for all samples and targeted an emission wavelength in the 900−950 nm range (AsH_3 pressure = 0.3 Torr). For the second dot (dot 2), the AsH_3 flow was varied for each sample (0.25 to 0.9 Torr). The growth time for each dot was 3.5 s, and the finished waveguide diameter was $D = 200$ nm. Figure 1b shows the photoluminescence (PL) spectra from the seven double-dot nanowires as well as from a single-dot reference sample, all measured at an excitation power $P = 0.25P_{sat}$, where P_{sat} is the excitation power required to saturate the ground-state transition in the reference sample.

Dot 1 is seen to emit at $\lambda \approx 920$ nm, with little variation from sample to sample (less than ±5 nm), highlighting the reproducibility of the growth process.[26] The emission wavelength of dot 2 varies from $\lambda \approx 900$ nm for 0.25 Torr to $\lambda \approx 1200$ nm for 0.6 Torr. The shift to longer wavelengths is accompanied by a dramatic decrease in the emission intensity, so much so that emission from dot 2 for 0.9 Torr is completely absent. For this dot, an emission wavelength of $\lambda = 1337$ nm was determined by pumping at $P = P_{sat}$.

To evaluate the emission properties of the InAsP/InP quantum dot nanowires, we have calculated the spontaneous emission rate into the fundamental HE_{11} nanowire waveguide mode ($\Gamma_{HE_{11}}$) for an electric dipole placed on the axis of the nanowire and oriented such that the dipole and nanowire axes are orthogonal (see details of the experimental methods).
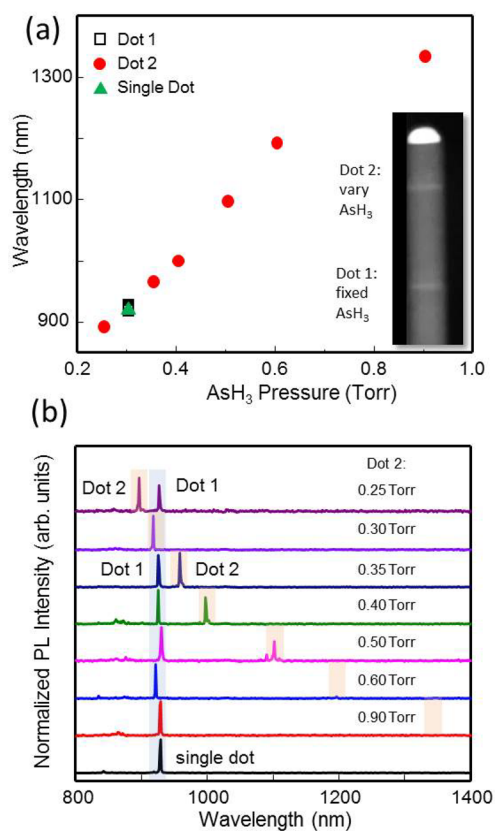
Figure 1. (a) Emission wavelength and (b) PL spectra of the double-dot system vs AsH_3 flux used for dot 2. The inset in panel a shows a transmission electron microscopy image of a double-dot nanowire core with an 18 nm diameter.

Emission rate data are presented in Figure 2 and are normalized to the calculated spontaneous emission rate in bulk InP, Γ_{bulk}, as a function of the normalized wire diameter, D/λ, as in ref 22. A normalized spontaneous emission rate into HE_{11} of close to $\Gamma_{HE_{11}} = 0.9$ can be achieved using an optimum waveguide
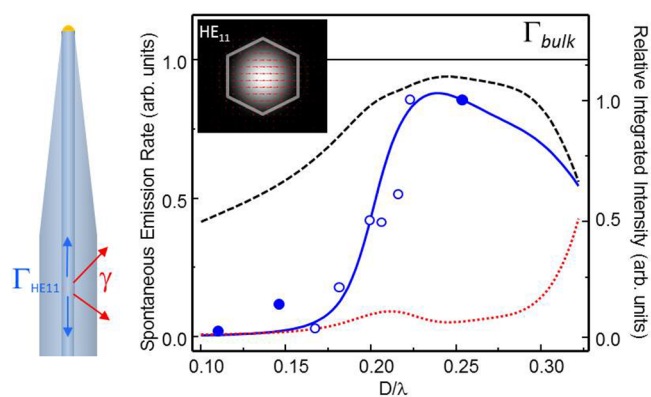

Figure 2. Calculated spontaneous emission rate into the fundamental HE_{11} nanowire waveguide mode ($\Gamma_{HE_{11}}$, blue solid line) and into leaky modes (γ, red dotted line) of an artificial atom placed on the axis of an InP nanowire as a function of the normalized wire diameter (D/λ). Black dashed line is $\beta = \Gamma_{HE_{11}}/(\Gamma_{HE_{11}} + \gamma)$. Open and filled circles are measured integrated PL intensities at saturation from dot 2 of the double-dot sample and the a-Si coated sample, respectively. Inset shows the calculated electric field intensity of one of the two orthogonally polarized HE_{11} modes.

diameter $D/\lambda \approx 0.23$. $\Gamma_{\mathrm{HE}_{11}}$ drops rapidly for smaller values of D/λ. For a dot emitting at $\lambda = 1360$ nm, for example, the optimal diameter is $D \approx 310$ nm. Using a standard nanowire waveguide optimized for $\lambda = 950$ nm, with a diameter of $D = 200$ nm, corresponds to $D/\lambda \approx 0.15$ at $\lambda = 1360$ nm and results in an emission rate that is reduced by a factor of 35 ($\Gamma_{\mathrm{HE}_{11}} = 0.024$). This reduction in spontaneous emission rate has two major effects: the saturated intensity of any given transition will be reduced as the radiative lifetime is increased,[23] and any competing nonradiative decay channels become more effective. An additional effect is a reduction in the fraction of photons coupled into the HE_{11} mode, β, versus all other radiation modes, in which $\beta = \Gamma_{\mathrm{HE}_{11}}/(\Gamma_{\mathrm{HE}_{11}} + \gamma)$ and γ is the emission rate into leaky modes. The value of β drops from 93% to 51% as D/λ changes from 0.23 to 0.15.

The combination of these effects can result in a dramatic decrease in the measured emission intensity when the photonic nanowire diameter is not optimized for the emission wavelength of interest. This decrease is observed directly in the measured spectra of Figure 1 and is included in Figure 2 (open circles) as the integrated intensity from dot 2 normalized to that of dot 1, where the intensities have been corrected for the wavelength-dependent detector efficiency. This data shows clear qualitative agreement with the predicted behavior as a function of D/λ.

To unambiguously demonstrate that the observed drop in PL intensity with increasing dot emission wavelength is influenced by the waveguide design, we repeatedly measure the same single-dot nanowire while increasing the diameter of the waveguide incrementally by depositing additional cladding material. The single dot was incorporated in a photonic nanowire with a diameter of $D = 150$ nm. The growth conditions were chosen to target an emission wavelength of $\lambda \approx 1350$ nm (AsH_3 pressure of 1.2 Torr and growth time of 3.5 s). Sequential coatings of amorphous silicon (a-Si) having a thickness $t_{\text{a-Si}}$ were then sputtered on the nanowire sidewall to incrementally increase the cladding diameter; see the inset of Figure 3a. InP and a-Si have similar indices of refraction at these wavelengths (3.2 and 3.4, respectively), and we assume that the a-Si cladding will simply increase the effective index of the waveguide and not affect the mode structure dramatically. Figure 3 shows the PL from a single dot as grown ($D = 150$ nm) after the deposition of $t_{\text{a-Si}} = 25$ nm ($D = 200$ nm) and after $t_{\text{a-Si}} = 75$ nm ($D = 350$ nm). With each coating, the PL intensity at saturation increases by close to an order of magnitude. The integrated intensities at saturation, normalized to that from the nanowire after the $t_{\text{a-Si}} = 75$ nm coating, are included in Figure 2 (filled circles). This data also shows clear qualitative agreement with the predicted behavior as a function of D/λ. We note that we also observe a slight red-shift of the emission wavelength with each a-Si coating. The sputtered a-Si on InP is compressively strained[27] and, hence, applies a tensile strain on the nanowire, resulting in a red-shift of the dot emission that depends on the thickness of the a-Si deposited.[28]

We look next at growing larger diameter waveguides tailored to the dot emission wavelength in situ rather than using an a-Si coating. The growth mode employed allows one to independently control the diameter of the nanowire core and that of the cladding.[9] One of the processing steps involved in the preparation of the growth substrate defines the opening in the SiO_2 mask that permits the selective-area growth of the cladding (see the Supporting Information). The size of this
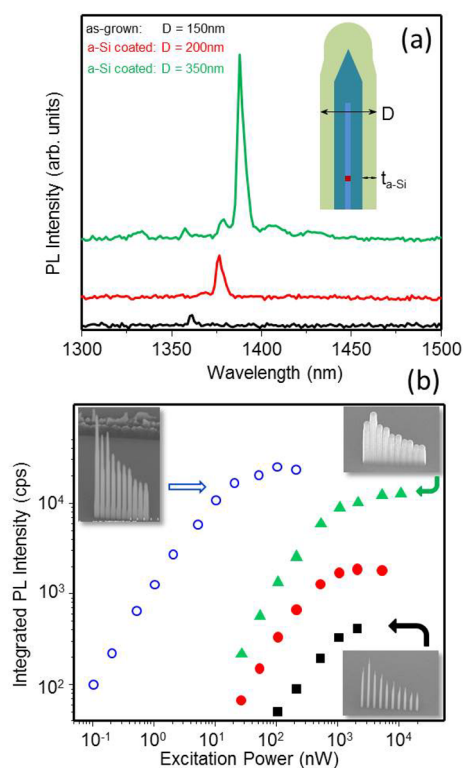

Figure 3. (a) PL spectra of the same nanowire as-deposited and coated with a-Si. (b) Corresponding integrated PL intensities of the ground-state emission: as-deposited: $t_{\text{a-Si}} = 0$ nm, $D = 150$ nm (black squares); first coat: $t_{\text{a-Si}} = 25$ nm, $D = 200$ nm (red circles); and second coat: $t_{\text{a-Si}} = 75$ nm, $D = 350$ nm (green triangles). Blue open circles correspond to the ground-state emission from a quantum dot in an all InP photonic nanowire having an as-deposited $D = 350$ nm. The two right-hand insets show scanning electron microscopy images of the same linear array of nanowires (400 nm pitch) as grown (top inset) and after the second a-Si coating (bottom inset). The left-hand inset shows an SEM image of a linear array of as-grown nanowires with $D = 350$ nm.

opening is determined by a hydrofluoric wet-etch, which, in turn, determines the diameter of the clad nanowire. For example, with an increase of the hole diameter from $D_{\text{hole}} = 100$ nm (12 s etch) to $D_{\text{hole}} = 300$ nm (24 s etch), the diameter of the clad nanowire increases from $D = 220$ nm to $D = 340$ nm.

We have used this control of the cladding diameter to design a waveguide tailored to the dot emission wavelength (e.g., $D/\lambda = 0.23$). We targeted an emission wavelength in the $\lambda = 1350$ nm range and a cladding diameter of $D = 350$ nm. To reach this wavelength, we tuned both the composition (increased AsH_3 flow) and degree of confinement (longer growth time) of the InAsP dot. In particular, the AsH_3 flow and growth time were 3 standard cubic centimeters per minute (sccm) and 9 s, respectively, compared to 2 sccm and 3 s for dots emitting at $\lambda = 950$ nm.[9] We employed a reduction of the confinement to shift the emission to longer wavelengths due to the difficulty in attaining arbitrarily high arsenic content in thinner dots as a consequence of phosphorus tailing at the growth interface (see details of the experimental methods). Figure 4a shows the power-dependent PL spectra of the device. The ground-state emission (X^-) is at $\lambda = 1342$ nm with a measured line width of ~150 μeV, limited by the resolution of the spectrometer.

The power-dependent integrated PL intensities extracted from Figure 4a are included in Figure 3 for comparison with the
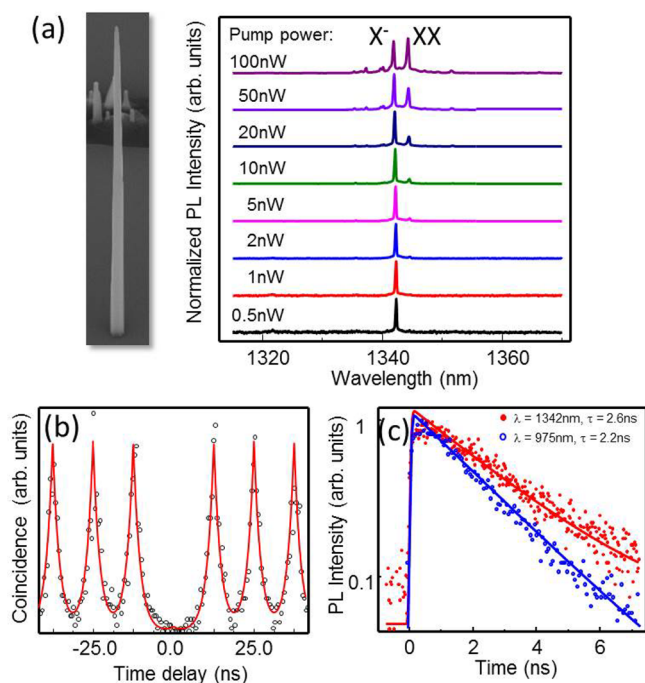
Figure 4. (a) Power-dependent spectra for a dot with a charged exciton ground-state emission $\lambda = 1342$ nm in a $D = 340$ nm waveguide shown in the inset ($D/\lambda = 0.25$). (b) Second-order correlation measurements of an emitter at 1310 nm. A $g^2(0) = 0.02$ is obtained from a fit to the data (red line). (c) Decay curves for two nanowire dots with the same normalized diameter but different ground-state emission wavelengths.

a-Si coated structures. There is a striking difference in the power required to saturate the ground-state transition between this sample and the a-Si coated sample of similar diameter. We speculate that this is related to the difference in absorption of the excitation laser and subsequent diffusion of carriers to the quantum dot between the two structures. The a-Si and its interface with the InP are likely trapping the majority of the optically generated carriers, resulting in an excitation power required for saturation that is close to 2 orders of magnitude larger.

The second difference concerns the count rate at saturation. The emission rate from the InP clad nanowire with $D = 340$ nm is almost 2 orders of magnitude higher than the device with $D = 150$ nm (35 kcps compared to 0.4 kcps). The emission rate for the $D = 340$ nm InP clad nanowire is also two times larger than the comparable a-Si clad nanowire, even though D/λ values are similar. The a-Si coating removes the taper present in the as-grown devices and one can expect a strong reduction in collection efficiency from both back-reflections at the nanowire tip and from increased divergence of the emitted light.[22,25] Also, a small amount of NIR absorption can be expected in unpassivated a-Si (see details of the experimental methods).

In Figure 4b, we show the second-order correlation measurement (see details of the experimental methods) of the charged exciton for a similar device from the same growth emitting at 1310 nm. Very pure single-photon emission is demonstrated by the absence of coincidence counts at a zero time delay. From a fit to the data, we determine a multiphoton emission probability of 2%, similar to devices operating in the 900–980 nm window.[9,18]

From a measurement of the decay of the X^- transition, we obtain a lifetime of $\tau = 2.6$ ns, similar to the lifetime of a nanowire dot emitting at $\lambda = 975$ nm with a similar normalized wire diameter. Both decay curves are shown in Figure 4c. These short lifetimes are consistent with an uninhibited emission process ($\tau \approx \tau_{\mathrm{bulk}}$); see Bulgarini et al.[23] Given the similar lifetimes, one would expect similar count rates from the sources at $\lambda = 975$ nm and $\lambda = 1342$ nm, assuming similar collection efficiencies (i.e., no difference in the far-field emission profile). The count rates at saturation from the two sources, taking account of the wavelength-dependent spectrometer efficiency, η, are 275 kilo counts per second (kcps) at $\lambda = 1342$ nm (measured 35 kcps; $\eta_{1310nm} = 12.7\%$) and 5900 kcps at $\lambda = 975$ nm (measured 135 kcps, $\eta_{980nm} = 2.3\%$).

The power radiated from an electric dipole is expected to scale as ω^4, corresponding to a count rate scaling as ω^3 (see the inset of Figure 5). Such behavior does not account for the large
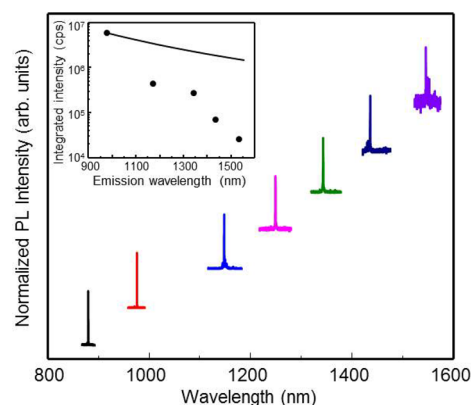
Figure 5. Normalized PL spectra of single InAsP/InP nanowire quantum-dot emitters in tailored photonic waveguides measured at an excitation power of 0.1 P_{sat}. Inset shows the emission-wavelength dependence of the count rate at the first lens (circles) as well as that of a radiating dipole (line).

emission intensity changes observed here when going to longer wavelengths. Nonradiative processes are also ruled out because we did not observe a significant change in lifetime or integrated PL intensity between 4 and 300 K for the dots emitting in the 1300 nm range. We are thus forced to consider the structural changes to the quantum dot that were used to shift the emission wavelength from $\lambda = 975$ nm to $\lambda = 1342$ nm. The AsH$_3$ flow was increased by 33%, and the growth time was tripled to 9 s. From TEM analysis of nanowire cores (see the Supporting Information), the longer quantum dot growth time increases the dot thickness from $h \approx 3$ nm to $h \approx 7$ nm. This corresponds to a much higher aspect ratio, $h/D_{\mathrm{dot}} = 7/18$, compared to typical self-assembled Stranski−Krastanow (SK) quantum dots ($h/D_{\mathrm{dot}} \approx 0.1$[29]). In SK dots, the strong confinement in the growth direction together, with the resulting strain profile, leads to a splitting of the heavy-hole (HH) and light-hole (LH) valence levels with a HH ground state.[29] Atomistic tight-binding calculations of similar InAs/InP quantum dot structures[30,31] have shown a transition from a compressive to tensile biaxial strain profile and a corresponding transition to a LH ground state with increasing quantum dot aspect ratio. This transition is expected to occur at intermediate quantum dot aspect ratios ($h/D_{\mathrm{dot}} \approx 0.8$[31]).

Considering the high aspect ratio of the quantum dots in our O-band emitters ($h/D_{\mathrm{dot}} \approx 0.4$), it is likely that the ground state

is a linear combination of HH and LH levels, producing a mixture of both perpendicular and parallel (with respect to the nanowire axis) polarized excitons.[29,31,32] Importantly, the latter is not expected to couple to the HE_{11} mode,[24] and the resulting radial emission would be collected with very low efficiency by the external optics. Thus, the increased fraction of recombination via the LH state from the increase in aspect ratio would result in unguided photons, contributing to the observed drop in count rates.

Finally, we show that with appropriately designed waveguide structures targeting $D/\lambda \approx 0.23$, the InAsP/InP nanowire quantum dot system can cover a large part of the NIR spectral range. Figure 5 shows PL spectra of single InAsP/InP quantum dot nanowires grown under different growth conditions. By adjusting the arsenic flow and dot thickness as well as the dot diameter,[33] this single material system can be tuned from $\lambda = 880$ nm to $\lambda = 1550$ nm. Each peak is resolution-limited and corresponds to a charged exciton (X^-) ground state. We note that the drop in the emission rate observed when going from $\lambda = 975$ nm to $\lambda = 1342$ nm continues as the wavelength is tuned further (see the inset of Figure 5), consistent with the mechanisms described above.

In conclusion, we have identified the design of the photonic nanowire waveguide as crucial in obtaining bright emission from InAsP/InP nanowire quantum dots emitting at telecom wavelengths. Using appropriately designed waveguides, we have demonstrated bright, narrow-line-width, single quantum dot emission from a single material system with an unprecedented tuning range spanning from 880 to 1550 nm. We observe a larger-than-expected decrease in brightness with increasing wavelength in these optimized structures and suggest that an increasing radial component of the quantum dot dipole due to valence band mixing between light- and heavy-hole levels may be a contributing factor.

Nanowire Growth. The growth of the InAsP/InP nanowire devices is carried out using chemical beam epitaxy on Fe-doped InP (111)B substrates with trimethylindium and precracked phosphine (PH_3) and arsine (AsH_3) as precursors of indium, phosphorus, and arsenic, respectively. A pair of growth systems were used, one in which the group V precursor flux is controlled directly using mass flow controllers and another in which the flux was set by a pressure control system. The growth temperature is controlled by band-edge thermometry and typically is in the range of 420−435 °C. The nanowires are grown using a combined selective-area and VLS process with Au catalyst particles (see refs 9 and 17 for details). Briefly, we first grow a nanowire core using a growth temperature and PH_3 flow tuned to obtain only axial growth via the VLS process (420−435 °C and 2 sccm, respectively). The quantum dot is incorporated in the core a few hundred nanometers from the base by switching AsH_3 in and PH_3 out of the growth chamber. The phosphorus present in the InAsP QD is due to a carry-over of phosphorus from the InP growth, the relative incorporation of which could be tuned by changing the AsH_3 flux. To grow the InP shell, the PH_3 flow is tripled to trigger radial growth and turn off the axial growth.

Amorphous Silicon Deposition. Ion-beam sputtering (Spector, Veeco) was used to deposit hydrogen-free a-Si at room temperature. The measured extinction coefficient of the films was $k \approx 0.01$ for wavelengths $\lambda = 1300−1400$ nm.

FDTD Calculations. Spontaneous emission rates were calculated using finite difference time domain (FDTD) with perfectly matched layer boundary conditions. Emission from an

electric dipole source located on the nanowire access was captured using a group of six planar detectors surrounding the nanowire. Coupling to the appropriate HE_{11} mode was assessed from an overlap integral on a plane with surface normal parallel to the nanowire axis.

Optical Spectroscopy. Optical measurements on individual nanowires were performed with the wires still attached to the (111)B InP substrate. The measurements were done at 4.2 K in a continuous flow helium cryostat using nonresonant, above band-gap excitation through a 50× microscope objective (NA = 0.42) with a ∼2 μm spot size. The PL was collected through the same microscope objective, dispersed using a 0.320 m grating spectrometer, and detected using a liquid-nitrogen cooled InGaAs diode array. Lifetime measurements were performed with pulsed excitation from a diode laser at 670 nm using 100 ps pulses at a repetition rate of 80 MHz, and the emitted photons were detected by a superconducting nanowire single-photon detector (SNSPD) from Single Quantum with a 40 ps timing jitter. Second-order correlation measurements were performed in a Hanbury Brown−Twiss setup using quasi-resonant excitation at 1255 nm with 2 ps pulses from an optical parametric oscillator at a repetition rate of 80 MHz. The single photons were detected using two single-quantum SNSPDs with a 30 ps timing jitter.

■ ASSOCIATED CONTENT

Ⓢ Supporting Information

The Supporting Information is available free of charge on the ACS Publications website at DOI: 10.1021/acs.nanolett.8b00550.

> Additional details and figures on additional PL measurements, TEM analysis of the quantum dot structure, and growth-substrate processing. (PDF)

■ AUTHOR INFORMATION

Corresponding Author

*E-mail: sofiane.haffouz@nrc.ca .Phone: 613-991-0761.

ORCID

Sofiane Haffouz: 0000-0003-1220-2622

Klaus D. Jöns: 0000-0002-5814-7510

Notes

The authors declare no competing financial interest.

■ REFERENCES

(1) Lo, H.-K.; Curty, M.; Qi, B. *Phys. Rev. Lett.* **2012**, *108*, 130503.

(2) Lo, H.-K.; Chau, H.-F. *Science* **1999**, *283*, 2050−2056.

(3) Aharonovich, I.; Englund, D.; Toth, M. *Nat. Photonics* **2016**, *10*, 631−641.

(4) Poole, P. J.; McCaffrey, J.; Williams, R. L.; Lefebvre, J.; Chithrani, D. *J. Vac. Sci. Technol., B: Microelectron. Process. Phenom.* **2001**, *19*, 1467−1470.

(5) Dalacu, D.; Mnaymneh, K.; Sazonova, V.; Poole, P.; Aers, G.; Lapointe, J.; Cheriton, R.; SpringThorpe, A.; Williams, R. L. *Phys. Rev. B: Condens. Matter Mater. Phys.* **2010**, *82*, 033381.

(6) Miyazawa, T.; Takemoto, K.; Sakuma, Y.; Hirose, S.; Usuki, T.; Yokoyama, N.; Takatsu, M.; Arakawa, Y. *J. J. Appl. Phys.* **2005**, *44*, L620.

(7) Kim, J.; Cai, T.; Richardson, C. J. K.; Leavitt, R.; Waks, E. *Optica* **2016**, *3*, 577−584.

(8) Birowosuto, M.; Sumikura, H.; Matsuo, S.; Taniyama, H.; van Veldhoven, P.; Nötzel, R.; Notomi, M. *Sci. Rep.* **2012**, *2*, 321.

(9) Dalacu, D.; Mnaymneh, K.; Lapointe, J.; Wu, X.; Poole, P.; Bulgarini, G.; Zwiller, V.; Reimer, M. *Nano Lett.* **2012**, *12*, 5919−5923.

(10) Lodahl, P.; Mahmoodian, S.; Stobbe, S. *Rev. Mod. Phys.* **2015**, *87*, 347.

(11) Claudon, J.; Bleuse, J.; Malik, N. S.; Bazin, M.; Jaffrennou, P.; Gregersen, N.; Sauvan, C.; Lalanne, P.; Gérard, J.-M. *Nat. Photonics* **2010**, *4*, 174.

(12) Borgström, M.; Zwiller, V.; Müller, E.; Imamoglu, A. *Nano Lett.* **2005**, *5*, 1439−1443.

(13) Reimer, M. E.; Bulgarini, G.; Akopian, N.; Hocevar, M.; Bavinck, M. B.; Verheijen, M. A.; Bakkers, E. P. A. M.; Kouwenhoven, L. P.; Zwiller, V. *Nat. Commun.* **2012**, *3*, 737.

(14) Heinrich, J.; Huggenberger, A.; Heindel, T.; Reitzenstein, S.; Höfling, S.; Worschech, L.; Forchel, A. *Appl. Phys. Lett.* **2010**, *96*, 211117.

(15) Dorenbos, S. N.; et al. *Appl. Phys. Lett.* **2010**, *97*, 171106.

(16) Holmes, M.; Choi, K.; Kako, S.; Arita, M.; Arakawa, Y. *Nano Lett.* **2014**, *14*, 982−986.

(17) Dalacu, D.; Kam, A.; Guy Austing, D.; Wu, X.; Lapointe, J.; Aers, G. C.; Poole, P. J. *Nanotechnology* **2009**, *20*, 395602.

(18) Reimer, M. E.; Bulgarini, G.; Fognini, A.; Heeres, R. W.; Witek, B. J.; Versteegh, M. A. M.; Rubino, A.; Braun, T.; Kamp, M.; Höfling, S.; Dalacu, D.; Lapointe, J.; Poole, P. J.; Zwiller, V. *Phys. Rev. B: Condens. Matter Mater. Phys.* **2016**, *93*, 195316.

(19) Jöns, K. D.; Schweickert, L.; Versteegh, M.; Dalacu, D.; Poole, P.; Gulinatti, A.; Giudice, A.; Zwiller, V.; Reimer, M. *Sci. Rep.* **2017**, *7*, 1700.

(20) Versteegh, M.; Reimer, M.; Jöns, K.; Dalacu, D.; Poole, P.; Gulinatti, A.; Giudice, A.; Zwiller, V. *Nat. Commun.* **2014**, *5*, 5298.

(21) Huber, T.; Predojević, A.; Khoshnegar, M.; Dalacu, D.; Poole, P.; Majedi, H.; Weihs, G. *Nano Lett.* **2014**, *14*, 7107−7114.

(22) Friedler, I.; Sauvan, C.; Hugonin, J. P.; Lalanne, P.; Claudon, J.; Gérard, J. M. *Opt. Express* **2009**, *17*, 2095.

(23) Bulgarini, G.; Reimer, M. E.; Hocevar, T. Z. M.; Bakkers, E. P. A. M.; Kouwenhoven, L. P.; Zwiller, V.; Zehender, T. *Appl. Phys. Lett.* **2012**, *100*, 121106.

(24) Jeannin, M.; Cremel, T.; Häyrynen, T.; Gregersen, N.; Bellet-Amalric, E.; Nogues, G.; Kheng, K. *Phys. Rev. Appl.* **2017**, *8*, 054022.

(25) Gregersen, N.; Nielsen, T. R.; Claudon, J.; Gérard, J.-M.; Mørk, J. *Opt. Lett.* **2008**, *33*, 1693−1695.

(26) Chen, Y.; Zadeh, I. E.; Jöns, K. D.; Fognini, A.; Reimer, M. E.; Zhang, J.; Dalacu, D.; Poole, P. J.; Ding, F.; Zwiller, V.; Schmidt, O. G. *Appl. Phys. Lett.* **2016**, *108*, 182103.

(27) Windischmann, H.; Collins, R.; Cavese, J. M. *J. Non-Cryst. Solids* **1986**, *85*, 261−272.

(28) Bavinck, M. B.; Zieliński, M.; Witek, B. J.; Zehender, T.; Bakkers, E. P. A. M.; Zwiller, V. *Nano Lett.* **2012**, *12*, 6206−6211.

(29) Korkusinski, M.; Hawrylak, P. *Phys. Rev. B: Condens. Matter Mater. Phys.* **2013**, *87*, 115310.

(30) Niquet, Y. M.; Mojica, D. *Phys. Rev. B: Condens. Matter Mater. Phys.* **2008**, *77*, 115316.

(31) Zieliński, M. *Phys. Rev. B: Condens. Matter Mater. Phys.* **2013**, *88*, 115424.

(32) Jeannin, M.; Artioli, A.; Rueda-Fonseca, P.; Bellet-Amalric, E.; Kheng, K.; André, R.; Tatarenko, S.; Cibert, J.; Ferrand, D.; Nogues, G. *Phys. Rev. B: Condens. Matter Mater. Phys.* **2017**, *95*, 035305.

(33) Dalacu, D.; Mnaymneh, K.; Wu, X.; Lapointe, J.; Aers, G. C.; Poole, P. J.; Williams, R. L. *Appl. Phys. Lett.* **2011**, *98*, 251101.